Flexible MnS–carbon fiber hybrids for lithium-ion and sodium-ion energy storage

Shuang Gao[a], Gang Chen[a,b], Yohan Dall'Agnese[a], Yingjin Wei[a], Zhongmin Gao[c], Yu Gao[a]*,

[a] Key Laboratory of Physics and Technology for Advanced Batteries (Ministry of Education), College of Physics, Jilin University, Changchun 130012, PR China
[b] State Key Laboratory of Superhard Materials, Jilin University, Changchun 130012, PR China
[c] State Key Laboratory of Inorganic Synthesis & Preparative Chemistry, Jilin University, Changchun 130012, Jilin, PR China
E-mail：yugao@jlu.edu.cn (Y. Gao）

Abstract

Nanostructures can improve battery capacity and cycle life, especially for sulfide materials. In this work, a freestanding flexible electrode of MnS nanoparticles embedded onto carbon nanofibers was prepared by electrospinning. The produced hybrid was used as electrode for lithium ion and sodium ion batteries. MnS nanoparticles have a size of about 5 nm and the particles are evenly distributed in the carbon nanofibers. Carbon nanofibers served as electronic conductor and buffer of the volume change. MnS nanoparticles react through rapid electrochemical reaction. As a Li-ion battery anode, this hybrid electrode exhibits specific capacity from 240 mAh g^{-1} at a high current density of 5 A g^{-1}, up to 600 mAh g^{-1} at 200 mA g^{-1}.

Keywords: Nanostructures; Manganese sulfide; Lithium ion battery; Sodium ion battery

1 Introduction

The exploration of low cost and environmentally friendly materials is essential to promote the development of the next generation of energy storage technology[1-3]. Current commercial batteries rely on lithium ion insertion mechanism into layered materials, such as graphite at the negative electrode[4-8]. Materials going through insertion mechanism have been extensively studied, however other charge storage mechanisms such as alloying, conversion or displacement reactions are still not

completely understood. Compared to graphite, which stores lithium ions through conversion reaction, most metal sulfides have higher theoretical specific capacity, but suffer from poor electronic conductivity and structural instability upon cycling[9-11]. In order to improve the cycle life and rate performance, a recognized strategy is to design a hybrid of the metal sulfide with an electronically conductive carbon-based framework. The addition of suitable carbon materials can greatly improve the electrical conductivity, the charge transfer, and the structural stability of these metal sulfides during cycling. In addition, the use of metal sulfide nanoparticles into porous carbon matrix can increase the surface area and improve the mechanical properties of the electrode[12-17]. Among the large family of metal sulfides, MnS is a relatively low-cost one[18,19] and has been investigated for various applications, including sensors, light-emitting diodes, solar cells, batteries and supercapacitors[20-23]. For lithium ion battery application, it has been proposed that MnS has a theoretical capacity of 616 mAh g^{-1} through conversion reaction. A wide variety of MnS nanostructures (e.g., nanospheres[24,25], nanowires[26], nanochains[27], and nanoparticles[28]) mixed with carbon black have been investigated as anode material. However, carbon black is not suitable to solve the issues related to the large volume change, thus other carbon materials must be proposed. Wu et al. proposed the synthesis of MnS nanoparticles embedded in porous carbon nanowires, which were located in 3D graphene matrix. That material delivered a reversible capacity of 660 mAh g^{-1} after five cycles at 0.5 A g^{-1}, which continuously decreased down to 526 mAh g^{-1} after 100 cycles[29]. Surprisingly, Xu et al. [30] and Liu et al. [18] reported capacities higher than the maximum theoretical capacity of MnS conversion reaction, approximately 800 mAh g^{-1} after 100 cycles at 0.5 A g^{-1} using MnS hollow microspheres on reduced graphene oxide sheets and 763 mAh g^{-1} after 100 cycles at 0.1 A g^{-1} using MnS crystallites grown on N-S co-doped reduced graphene oxide, respectively. While these various graphene-MnS hybrid results have been reported, little noteworthy effort was made on other types of hybrid. hybrid electrodes made of carbon fibers embedded with MnS nanoparticles could improve the electrical

conductivity of the electrode, buffer volume changes, and form a porous 3D structure beneficial for electrode/electrolyte interface and mechanical stability [25,27,29-35].

In this paper, we synthesized a freestanding flexible electrode of MnS nanoparticles embedded onto carbon nanofibers by electrospinning and investigated its electrochemical performances for lithium-ion and sodium-ion energy storage applications.

2 Experimental

2.1 Material synthesis

0.7 g of polyacrylonitrile (PAN, Aldrich, USA) was dissolved in 10 mL of N-dimethylformamide (DMF) at 80 ^{o}C for 2 h under magnetic stirring. 0.14 mg manganese sulfate monohydrate ($MnSO_4 \cdot H_2O$) was added into the PAN solution and stirred overnight. The resulting solution was transferred to a plastic syringe with stainless steel needle for the electrospinning process. The distance between the needle and the aluminum current collector was maintained at 20 cm and a direct current voltage of 15 kV was applied. The flow rate of the precursor solution was fixed at approximately 0.3 mL h^{-1}. After the electrospinning, a white film was obtained and peeled off from the aluminum current collector. The film was heated at 2 ^{o}C min^{-1} to 280 ^{o}C for 5 h in a muffle furnace, then at 2 ^{o}C min^{-1} to 700 ^{o}C for 2 h under N_2 atmosphere in a tube furnace. The black freestanding film obtained is labeled MnS@CNF. For comparison, the same protocol was performed without manganese sulfate monohydrate to obtain a freestanding flexible carbon nanofiber film without MnS, noted CNF.

2.2 Characterization

Crystal structures were investigated using a Dandong Haoyuan DX-2700B X-ray diffractometer equipped with Cu-Kα radiation source. Raman spectrum was collected via a Renishaw spectrometer with an argon laser (wavelength of 514.53 nm). X-ray photoelectron spectroscopy (XPS) was performed using a VG Scientific ESCALAB 250 spectrometer and peaks fitting was carried out using Origin. Field emission

scanning electron microscope (FE-SEM, HITACHI SU8020) and transmission electron microscopy (TEM, JEOL JEM-2200FS) were used to observe the sample morphologies. Nitrogen sorption analysis was performed at 77 K using Kubo-X1000 apparatus after outgassing under vacuum at 120 °C for 2 h. The specific surface area and the pore-size distribution were calculated using the Brunauer−Emmett−Teller (BET) method and the Horvath-Kawazoe algorithm, respectively.

2.3 Electrochemical measurement

The electrochemical performance was investigated using 2032-type coin cells assembled in an argon-filled glovebox. The freestanding films were cut into 0.64 cm^2 rectangles with mass loadings of 1.25 mg cm^{-2} for MnS@CNF. Then they were directly used as the working electrode without adding binder or conductive additives. For lithium ion battery test, 1 M $LiPF_6$ in a mixture of ethylene carbonate (EC) and diethyl carbonate (DEC) (1:1 in weight) was used as the electrolyte and lithium foil was used as the counter and reference electrode. For sodium ion battery test, 1 M $NaClO_4$ in a mixture of ethylene carbonate (EC) and propylene carbonate (PC) (1:1 v/v) was used as the electrolyte and metallic sodium was used as the counter and reference electrode. The working and counter electrodes were separated by a Celgard 2400 membrane and Whatman glass microfiber filters for lithium ion battery test and sodium ion battery respectively. Cyclic voltammetry (CV) measurements were performed on a Bio-Logic VSP potentiostat. Galvanostatic charge-discharge measurements were conducted using a LANHE CT2001A at various current densities.

3 Results and discussion

The preparation procedure of MnS@CNF film is schematically shown in Figure 1. First, continuous polymer nanofiber webs containing dissolved $MnSO_4$ are prepared by electrospinning, a low-cost and scalable approach for forming long polymer fibers. The fibers are collected as a freestanding film thanks to the formation of a randomly oriented fiber network. Then, the flexible MnS@CNF electrode is obtained through a two-step heat treatment process. In the first step, the as-spun film

is heated in air at 280 °C to remove absorbed water and solvent. In the second step, the film is carbonized in an N_2 atmosphere at 700 °C. During the carbonization process, the PAN polymer backbones turn into carbon nanofibers and $MnSO_4$ particles react to form MnS particles. The electrode contains 16 wt % of MnS, as determined by TGA (Figure S1).

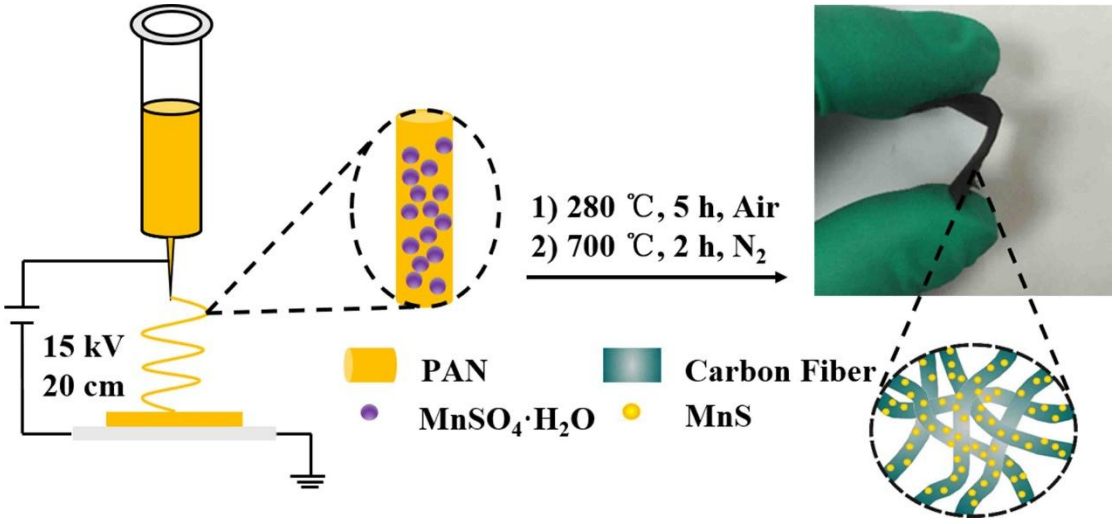

Figure 1. Schematic illustration of the synthesis of MnS@CNF and a digital photo of the flexible freestanding electrode.

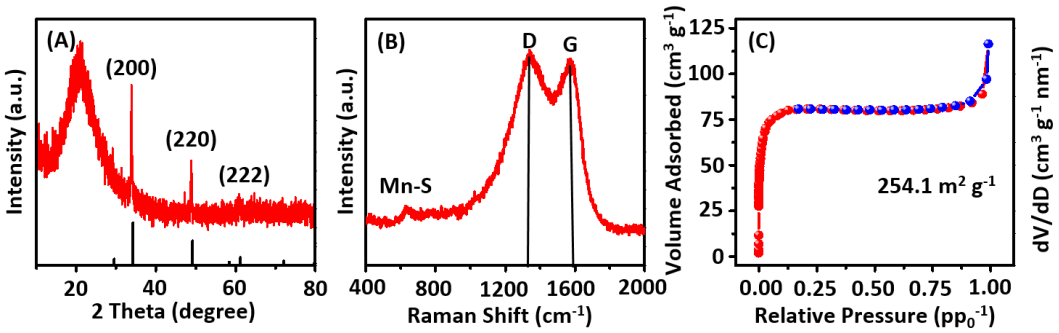

Figure 2. (A) X-ray diffraction pattern (B) Raman spectra of MnS@CNF. (C) Nitrogen adsorption/desorption isotherms of MnS@CNF.

Figure 2A shows the X-ray diffraction pattern of the as-synthesized MnS@CNF films. The diffraction peaks at 34.20° and 49.14° are attributed to the cubic phase of MnS. The crystal size of MnS is calculated to be about 5 nm using the Scherrer formula. The broad diffraction peak at about 21° is attributed to amorphous carbon.

Figure 2B presents the Raman spectra of the as-prepared hybrid between 100 and 2000 cm^{-1}. The Raman scattering peak observed at 639 cm^{-1} can be assigned to the MnS. The characteristic peaks around 1341 and 1574 cm^{-1} in the Raman spectrum of the hybrid materials are assigned to the D band and G band from PAN[31,36]. The Raman I_D/I_G ratio is widely used to evaluate the quality of carbon materials. The hybrid materials' I_G/I_D value is calculated to be greater than one. From the Raman results, we see that MnS@CNF composite materials have a large number of defects and a disordered structure. This provides extra sites for Li^+/Na^+ storage, thus effectively improving the specific capacity and rate capability. XPS spectra of MnS@CNF are shown in Figure S2 and are consistent with the XRD and Raman results. Nitrogen adsorption measurements of the MnS@CNF (Figure 2C) were performed to determine the specific surface area of the electrode material. Using Brunauer-Emmett-Teller method, a specific surface area of 254 $m^2\ g^{-1}$ and a total pore volume of 0.18 $cm^3\ g^{-1}$ were calculated. The pore size was calculated to be in the range of 0.4 to 2 nm, indicating micropores in the carbon nanofibers of the MnS@CNF film (Figure S3).

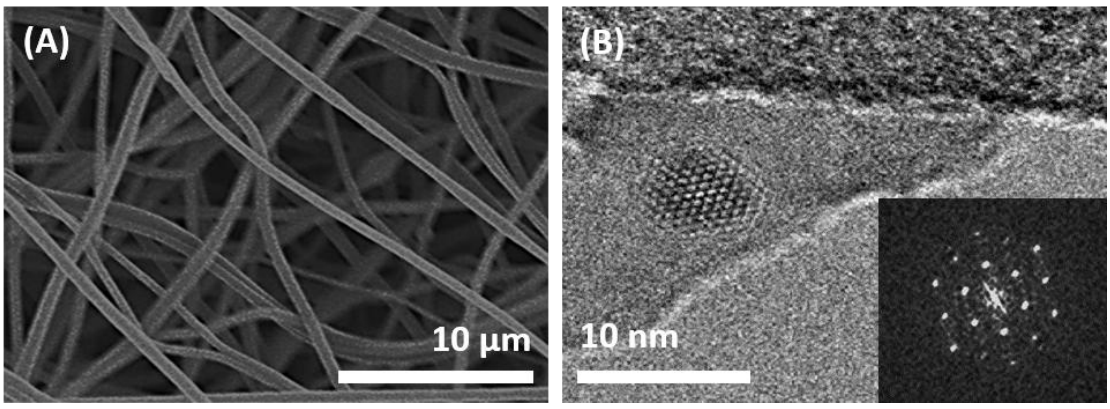

Figure 3. (A) SEM image, (B) HRTEM image and its corresponding selected area FFT pattern (inset) of the MnS@CNF electrode.

Figure S4 and Figure 3A show scanning electron microscopy images (SEM) of freestanding films before and after the carbonization step, respectively. The films have similar morphology, consisting of a 3D network of interconnected fibers without aggregation. The fiber diameter is about 500 nm. SEM of the cross section of the

MnS@CNF film (Figure S5) shows that the film is approximately 13 μm thick. Figure 3B shows a transmission electron microscopy (TEM) image of MnS@CNF. The corresponding 2D fast Fourier transform (FFT) pattern exhibited the typical hexagonal structure of MnS. The FFT paterns confirms that nanoscale MnS particles were successfully prepared. MnS nanoparticles are less than 10 nm large and uniformly embedded in the carbon matrix. No lattice fringes of graphitic carbon are observed, confirming the amorphous nature of the carbon fiber. Figure S6 shows the elemental distribution of C, Mn and S elements in the MnS@CNF hybrid electrode by Energy-dispersive X-ray spectroscopy mapping. It can be seen that the C, Mn and S elements are evenly distributed in the carbon nanofibers.

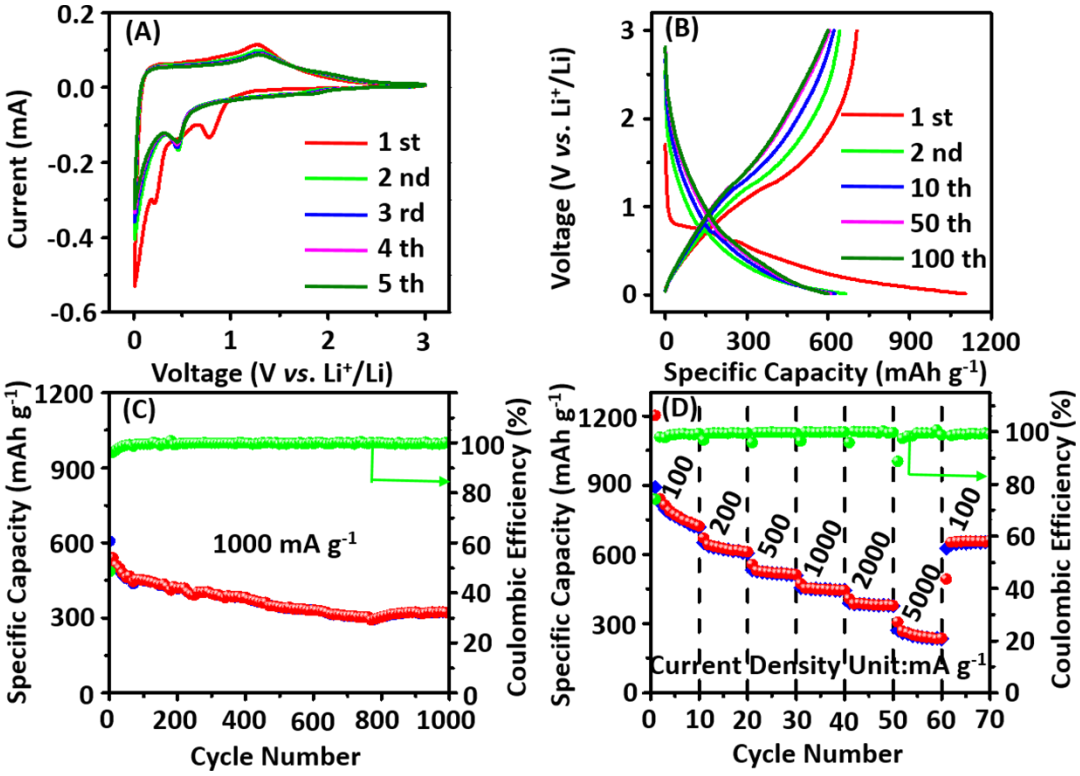

Figure 4. Electrochemical performance of the MnS@CNF electrode for lithium ion storage. (A) Cyclic voltammograms at a scan rate of 0.1 mV s^{-1}. (B) Galvanostatic charge−discharge profile at 200 mA g^{-1}. (C) Long-term cycle stability at 1000 mA g^{-1}. (D) Rate performance at various current densities.

The electrochemical properties of the MnS@CNF electrodes for lithium storage are shown in Figure 4. Note that the current density and specific capacity are based on

the mass of the whole electrode. Figure 4A shows the five first cycles obtained by cyclic voltammetry (CV) at a scan rate of 0.1 mV s^{-1}. To clarify the electrochemical reaction occurring, it can be noted that the electrochemical behavior of MnS@CNF electrodes is mainly attributed to MnS because the cyclic voltammogram of pure CNF does not contain any of the observed redox peak (Figure S7). In the first reduction of MnS@CNF, there are two peaks at about 0.1 V and 0.7 V, which can be attributed to the formation of a solid electrolyte interface (SEI) layer and Li^+ insertion into the MnS lattice because these peaks disappear in the subsequent cycles. The positions of reduction and oxidation peaks, at 0.45 V and 1.25 V respectively, are reversible in the following cycles. These peaks indicate that stable electrochemical reactions between MnS and Li^+ occur, which is proposed to be a conversion reaction in the literature [32].

The discharge–charge curves of the MnS@CNF electrode for the 1st, 2 nd, 10 th, 50 th and 100 th cycles at a constant current density of 200 mA g^{-1} in the voltage range of 0.01 –3.0 V are displayed in Figure 4B. Figure S8 shows the corresponding cycling performances for 100 cycles. The MnS@CNF had an initial discharge capacity of 1104 mAh g^{-1}, and corresponding initial Coulombic efficiencies of 64 %. The low initial columbic efficiency is attributed to the formation of the SEI layer and decomposition of the electrolyte, similar to that reported in other metal oxides and sulfide anode materials of lithium-ion batteries [31,37]. The subsequent cycles show good reversibility and the discharge capacity remains at 598 mAh g^{-1} even after 100 cycles, indicating the good cycling stability of the MnS@CNF electrode. Similar to other MnS hybrid reported [18,30], the capacity achieved is superior to our expectation and is attributed to the synergistic effects between the 3D architecture: the nanosized MnS and the high porosity of the carbon nanofiber. Interestingly, the charge-discharge curves show no well-defined voltage plateau at the previously mentioned oxidation and reduction potentials, on contrary to previously reported work on MnS. This is due to the use of nanoparticle MnS instead of bulk particles. Indeed, a battery-type material (well-defined voltage plateau) can exhibit pseudocapacitive behavior (linear response) if it is scaled down to nanoparticles [38,39]. Therefore, the

MnS@CNF hybrid might be more suitable for lithium ion capacitor than lithium ion battery.

The MnS@CNF exhibits remarkable long-life cycling performance at high current densities (1000 mA g^{-1}), as shown in Figure 4C. The initial discharge capacity is 1250 mAh g^{-1}, 374 mAh g^{-1} after 50 cycles, and 257 mAh g^{-1} after 1000 cycles. The SEM image obtained after 100 cycles (Figure S9) confirms that the 3D structure is still porous and open for easy Li^+ diffusion, even though the fiber appears thicker due to SEI coating and volume expansion. The nanoscale architecture of MnS@CNF increases its conductivity, reduces the diffusion distance of Li^+, increases the effective interface area, contributes to faster charge transfer, avoids the aggregation of nanoparticles, and effectively adapts to large volume expansion greatly improving the reversibility of MnS lithiation.

Rate capability is a vital evaluation factor for high performance of LIBs and lithium ion capacitors. Figure 4D displays the rate performance of the MnS@CNF hybrid at different current densities. The MnS@CNF have exhibited high rate performance. The discharge specific capacities of the MnS@CNF can be around 723, 610, 512, 445, 379 and 237 mAh g^{-1} at 100, 200, 500, 1000, 2000 and 5000 mA g^{-1}, respectively. The latter corresponds to a high energy density of 384 Wh kg^{-1} at the high power density of 7768 W kg^{-1}. When the current density returns to 100 mA g^{-1}, the MnS@CNF electrode can recover a specific capacity up to 658 mA h g^{-1}. It demonstrates that this architecture exhibits good electrochemical stability at high rates.

Figure 5 shows a series of electrochemical measurements performed in order to evaluate the sodium storage capacity of the MnS@CNF hybrid. The cyclic voltammograms (Figure 5A) do not display any redox peaks, except those associated to SEI formation during the first reduction. Although without proof, it has been proposed that MnS stores sodium through conversion reaction, similar to lithium [31]. In our case, there is also a contribution from the sodiation of carbon nanofibers.

The galvanostatic charge-discharge curves at 20 mA g^{-1} (Figure 5B) are consistent with the CV curves, with linear voltage response. The MnS@CNF

electrode provides a specific capacity of 580 mAh g^{-1} in the first cycle of discharge, with an initial coulombic efficiency of 38 % due to SEI formation. Following cycles show good reversibility (Figure 5B and Figure 5C) and a stable capacity of 220 mAh g^{-1} remained after 200 cycles. In addition, the rate capability test at various current densities (Figure 5D) shows good capacity retention. The MnS@CNF electrode provides an average capacity of 220, 177, 152, 132, 107 and 87 mAh g^{-1} at 20, 50, 100, 200, 500 and 1000 mA g^{-1}, respectively. These good performances are attributed to the suitable electrode design. As discussed earlier, the 3D structure with embedded MnS nanoparticles provides more active sites for rapid Na^+ diffusion and good electrolyte availability for all electroactive surfaces. These results correspond to reasonable energy density of 129 Wh kg^{-1} at a power density of 1480 W kg^{-1} and calculate it for 87 mAh g^{-1} at 1000 mA g^{-1}.

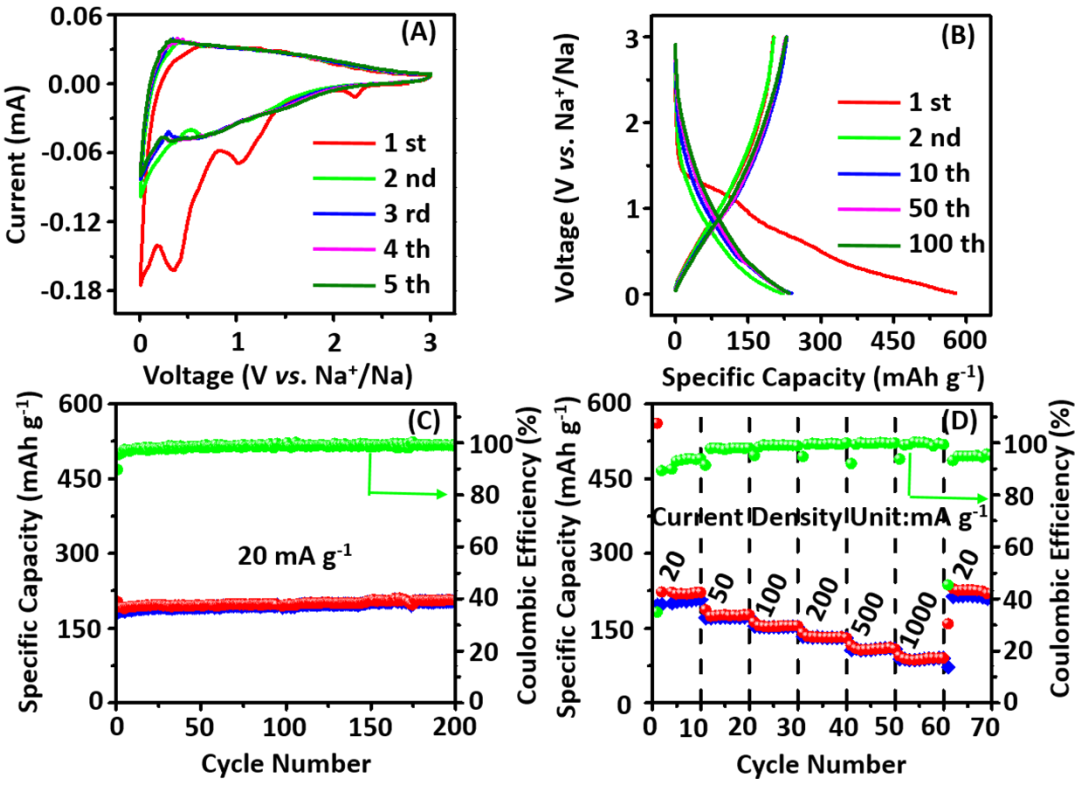

Figure 5. Electrochemical performance for sodium storage. (A) Cyclic voltammogram curves of the MnS@CNF electrode for the initial 5 cycles at a scanning rate of 0.1 mV s^{-1} in the voltage range of 0.01 - 3V. (B) Galvanostatic discharge–charge profiles

for different cycles at a current density of 20 mA g^{-1} in the voltage range of 0.01 – 3V. (C)Cycling performance of MnS@C electrode and the corresponding coulombic efficiency at 20 mA g^{-1}. (D) Rate capability at various current densities from 20 to 1000 mA g^{-1}.

4 Conclusions

In summary, MnS nanoparticles are embedded in carbon nanofibers by electrospinning and thermal treatment. The proposed method is simple, cheap and can be mass produced. The prepared hybrid material does not require any binder or conductive additives and can directly be used as electrode for lithium ion or sodium ion energy storage, facilitating the assembly process. The hybrid was electrochemically tested as anode materials and exhibited high reversible capacity and long cycle life upon Li^+ and Na^+ storage. It could be of interest as electrode material for metal-ion capacitors, as good rate performances were observed, 240 mAh g^{-1} at 5 A g^{-1} (< 3 min charge) through lithium ion storage and 87 mAh g^{-1} at 1 A g^{-1} (5 min charge) through sodium ion storage, respectively. These performances were attributed to an open 3D architecture, consisting of MnS nanoparticles embedded in a conductive network of interconnected carbon nanofibers, enabling rapid redox reaction, reducing the ions diffusion distance, increasing the conductivity, and being unaffected by the volume change.

Acknowledgements

This research was financially supported by the Ministry of Science and Technology of China (No. 2015CB251103). Jilin Province/Jilin University Co-construction Project – Funds for New Materials (SXGJSF2017-3). This work was supported by Yury Gogotsi acknowledge the Thousand Talents program (China). Open Project of State Key Laboratory of Superhard Materials (Jilin University, No. 201513), State Major Scientific Instrument and Equipment Development of China (No. 2012YQ24026407). Thank Professor Yury for his participation in the discussion of the article.

References

[1] Y. Wang, G. Cao, Developments in nanostructured cathode materials for high-performance lithium-ion batteries, Advanced Materials 20 (2008) 2251-2269.

[2] D. Kundu, E. Talaie, V. Duffort, L.F. Nazar, The Emerging Chemistry of Sodium Ion Batteries for Electrochemical Energy Storage, Angewandte Chemie-International Edition 54 (2015) 3431-3448.

[3] C. Chen, Y. Wen, X. Hu, X. Ji, M. Yan, L. Mai, P. Hu, B. Shan, Y. Huang, Na+ intercalation pseudocapacitance in graphene-coupled titanium oxide enabling ultra-fast sodium storage and long-term cycling, Nature Communications 6 (2015) 1-8.

[4] H. Pan, Y.-S. Hu, L. Chen, Room-temperature stationary sodium-ion batteries for large-scale electric energy storage, Energy & Environmental Science 6 (2013) 2338-2360.

[5] P.G. Bruce, S.A. Freunberger, L.J. Hardwick, J.-M. Tarascon, Li-O_2 and Li-S batteries with high energy storage, Nature Materials 11 (2012) 19-29.

[6] N.-S. Choi, Z. Chen, S.A. Freunberger, X. Ji, Y.-K. Sun, K. Amine, G. Yushin, L.F. Nazar, J. Cho, P.G. Bruce, Challenges Facing Lithium Batteries and Electrical Double-Layer Capacitors, Angewandte Chemie-International Edition 51 (2012) 9994-10024.

[7] T. Zhu, C.K.N. Peh, M. Hong, G.W. Ho, Outside-In Recrystallization of ZnS-$Cu_{1.8}S$ Hollow Spheres with Interdispersed Lattices for Enhanced Visible Light Solar Hydrogen Generation, Chemistry-a European Journal 20 (2014) 11505-11510.

[8] J. Liu, K. Song, P.A. van Aken, J. Maier, Y. Yu, Self-Supported $Li_4Ti_5O_{12}$-C Nanotube Arrays as High-Rate and Long-Life Anode Materials for Flexible Li-Ion Batteries, Nano Letters 14 (2014) 2597-2603.

[9] Y.-X. Wang, J. Yang, S.-L. Chou, H.K. Liu, W.-x. Zhang, D. Zhao, S.X. Dou, Uniform yolk-shell iron sulfide-carbon nanospheres for superior sodium-iron sulfide batteries, Nature Communications 6 (2015) 1-9.

[10] Z. Hu, L. Wang, K. Zhang, J. Wang, F. Cheng, Z. Tao, J. Chen, MoS_2 Nanoflowers with Expanded Interlayers as High-Performance Anodes for Sodium-Ion Batteries, Angewandte Chemie-International Edition 53 (2014) 12794-12798.

[11] S.-B. Son, T.A. Yersak, D.M. Piper, S.C. Kim, C.S. Kang, J.S. Cho, S.-S. Suh, Y.-U. Kim, K.H. Oh, S.-H. Lee, A Stabilized PAN-FeS_2 Cathode with an EC/DEC Liquid Electrolyte, Advanced Energy Materials 4 (2014) 1-5.

[12] S. Park, J. An, I. Jung, R.D. Piner, S.J. An, X. Li, A. Velamakanni, R.S. Ruoff, Colloidal Suspensions of Highly Reduced Graphene Oxide in a Wide Variety of Organic Solvents, Nano Letters 9 (2009) 1593-1597.

[13] Z.-S. Wu, G. Zhou, L.-C. Yin, W. Ren, F. Li, H.-M. Cheng, Graphene/metal oxide hybrid electrode materials for energy storage, Nano Energy 1 (2012) 107-131.

[14] Y. Fu, A. Manthiram, Silicon nanoparticles supported on graphitic carbon paper as a hybrid anode for Li-ion batteries, Nano Energy 2 (2013) 1107-1112.

[15] S. Peng, X. Han, L. Li, Z. Zhu, F. Cheng, M.U. Srinivansan, S. Adams, S. Ramakrishna, Unique Cobalt Sulfide/Reduced Graphene Oxide Composite as an Anode for Sodium-Ion Batteries with Superior Rate Capability and Long Cycling Stability, Small 12 (2016) 1359-1368.

[16] Y. Tang, T. Chen, S. Yu, Morphology controlled synthesis of monodispersed manganese sulfide nanocrystals and their primary application in supercapacitors with high performances, Chemical Communications 51 (2015) 9018-9021.

[17] X. Wei, W. Li, J.-a. Shi, L. Gu, Y. Yu, FeS@C on Carbon Cloth as Flexible Electrode for Both Lithium and Sodium Storage, Acs Applied Materials & Interfaces 7 (2015) 27804-27809.

[18] Y. Liu, Y. Qiao, W.-X. Zhang, Z. Li, X.-L. Hu, L.-X. Yuan, Y.-H. Huang, Coral-like alpha-MnS composites with N-doped carbon as anode materials for high-performance lithium-ion batteries, Journal of Materials Chemistry 22 (2012) 24026-24033.

[19] J.M. Yan, H.Z. Huang, J. Zhang, Z.J. Liu, Y. Yang, A study of novel anode material CoS_2 for lithium ion battery, Journal of Power Sources 146 (2005) 264-269.

[20] X. Li, J. Shen, N. Li, M. Ye, Fabrication of gamma-MnS/rGO composite by facile one-pot solvothermal approach for supercapacitor applications, Journal of Power Sources 282 (2015) 194-201.

[21] C. Zhu, X. Mu, P.A. van Aken, Y. Yu, J. Maier, Single-Layered Ultrasmall Nanoplates of MoS2 Embedded in Carbon Nanofibers with Excellent Electrochemical Performance for Lithium and Sodium Storage, Angewandte Chemie-International Edition 53 (2014) 2152-2156.

[22] B. Yang, X. Zuo, P. Chen, L. Zhou, X. Yang, H. Zhang, G. Li, M. Wu, Y. Ma, S. Jin, X. Chen, Nanocomposite of Tin Sulfide Nanoparticles with Reduced Graphene Oxide in High-Efficiency Dye-Sensitized Solar Cells, ACS Applied Materials & Interfaces 7 (2015) 137-143.

[23] M. Pumera, Z. Sofer, A. Ambrosi, Layered transition metal dichalcogenides for electrochemical energy generation and storage, Journal of Materials Chemistry A 2 (2014) 8981-8987.

[24] P. Jin, X. Zhang, J. Wang, Mesoporous gamma-MnS nanospheres as anode materials for Li ion batteries, Materials Letters 188 (2017) 13-16.

[25] L. Fei, B.P. Williams, S.H. Yoo, J.M. Carlin, Y.L. Joo, A general approach to fabricate free-standing metal sulfide@carbon nanofiber networks as lithium ion battery anodes, Chemical Communications 52 (2016) 1501-1504.

[26] J. Beltran-Huarac, O. Resto, J. Carpena-Nunez, W.M. Jadwisienczak, L.F. Fonseca, B.R. Weiner, G. Morell, Single-Crystal gamma-MnS Nanowires Conformally Coated with Carbon, Acs Applied Materials & Interfaces 6 (2014) 1180-1186.

[27] J. Ning, D. Zhang, H. Song, X. Chen, J. Zhou, Branched carbon-encapsulated MnS core/shell nanochains prepared via oriented attachment for lithium-ion storage, Journal of Materials Chemistry A 4 (2016) 12098-12105.

[28] M.S. Javed, X. Han, C. Hu, M. Zhou, Z. Huang, X. Tang, X. Gu, Tracking Pseudocapacitive Contribution to Superior Energy Storage of MnS Nanoparticles Grown on Carbon Textile, ACS Applied Materials & Interfaces 8 (2016) 24621-24628.

[29] C. Wu, J. Maier, Y. Yu, Generalizable Synthesis of Metal-Sulfides/Carbon Hybrids with Multiscale, Hierarchically Ordered Structures as Advanced Electrodes for Lithium Storage, Advanced Materials 28 (2016) 174-180.

[30] D. Chen, H. Quan, X. Luo, S. Luo, 3-D graphene cross-linked with mesoporous MnS clusters with high lithium storage capability, Scripta Materialia 76 (2014) 1-4.

[31] X. Xu, S. Ji, M. Gu, J. Liu, In Situ Synthesis of MnS Hollow Microspheres on Reduced Graphene Oxide Sheets as High-Capacity and Long-Life Anodes for Li- and Na-Ion Batteries, Acs Applied Materials & Interfaces 7 (2015) 20957-20964.

[32] Y. Hao, C. Chen, X. Yang, G. Xiao, B. Zou, J. Yang, C. Wang, Studies on intrinsic phase-dependent electrochemical properties of MnS nanocrystals as anodes for lithium-ion batteries, Journal of Power Sources 338 (2017) 9-16.

[33] D. Xu, R. Jiao, Y. Sun, D. Sun, X. Zhang, S. Zeng, Y. Di, L-Cysteine-Assisted Synthesis of Urchin-Like gamma-MnS and Its Lithium Storage Properties, Nanoscale Research Letters 11 (2016).

[34] J. S. Atchison, D. Tadros, Y. Gogotsi, P. Holt, W. A. Stoy, J. A. Kots, C. L. Schauer, in 2012 ASEE Annual Conference, Amer. Soc. Engineering Education, Washington, 2012.

[35] L. Zhang, L. Zhou, H.B. Wu, R. Xu, X.W. Lou, Unusual Formation of Single-Crystal Manganese Sulfide Microboxes Co-mediated by the Cubic Crystal Structure and Shape, Angewandte Chemie-International Edition 51 (2012) 7267-7270.

[36] K.N. Kudin, B. Ozbas, H.C. Schniepp, R.K. Prud'homme, I.A. Aksay, R. Car, Raman spectra of graphite oxide and functionalized graphene sheets, Nano Letters 8 (2008) 36-41.

[37] J. Cabana, L. Monconduit, D. Larcher, M. Rosa Palacin, Beyond Intercalation-Based Li-Ion Batteries: The State of the Art and Challenges of Electrode Materials Reacting Through Conversion Reactions, Advanced Materials 22 (2010) 170-192.

[38] P. Simon, Y. Gogotsi, B. Dunn, Where Do Batteries End and Supercapacitors Begin?, Science 343 (2014) 1210-1211.

[39] T. Brousse, D. Belanger, J.W. Long, To Be or Not To Be Pseudocapacitive?, Journal of the Electrochemical Society 162 (2015) 5185-5189.